DEVELOPING AND EXPLOITING A UNIQUE SEISMIC DATASET FROM SOUTH AFRICAN GOLD MINES FOR SOURCE CHARACTERIZATION AND WAVE PROPAGATION

Jordi Julià[1], Andrew A. Nyblade[1], Rengin Gök[2], William R. Walter[2], Lindsay Linzer[3], and Ray Durrheim[3]

Penn State University[1], Lawrence Livermore National Laboratory[2], and
Council for Scientific and Industrial Research[3]

Sponsored by National Nuclear Security Administration

Contract Nos. DE-FC52-06NA27320 and DE-AC52-07NA27344
Proposal No. BAA06-06

ABSTRACT

In this project, we are developing and exploiting a unique seismic dataset to address the characteristics of small seismic events and the associated seismic signals observed at local (<200 km) and regional (<2000 km) distances. The dataset is being developed using mining-induced events from three deep gold mines in South Africa recorded on in-mine networks (<1 km) composed of tens of high-frequency sensors, a network of four broadband stations installed as part of this project at the surface around the mines (1–10 km), and a network of existing broadband seismic stations at local/regional distances (50–1000 km) from the mines. After a year of seismic monitoring of mine activity (2007), over 10,000 events in the range $-3.4 < ML < 4.4$ have been catalogued and recorded by the in-mine networks. Events with positive magnitudes are generally well recorded by the surface-mine stations, while magnitudes of 3.0 and larger are seen at regional distances (up to ~600 km) in high-pass filtered recordings.

We have analyzed in-mine recordings in detail at one of the South African mines (Savuka) to (i) improve on reported hypocentral locations, (ii) verify sensor orientations, and (iii) determine full moment tensor solutions. Hypocentral relocations on all catalogued events have been obtained from P- and S-wave travel-times reported by the mine network operator through an automated procedure that selects travel times falling on Wadati lines with slopes in the 0.6–0.7 range; sensor orientations have been verified and, when possible, corrected by correlating P-, SV-, and SH-waveforms obtained from theoretical and empirical (polarization filter) rotation angles; full-moment tensor solutions have been obtained by inverting P-, SV-, and SH-spectral amplitudes measured on the theoretically rotated waveforms with visually assigned polarities. The relocation procedure has revealed that origin times often necessitate a negative correction of a few tenths of a second and that hypocentral locations may move a few hundreds of meters. The full moment tensor determination has revealed that the most common focal mechanism (47 out of 82 solutions for events in the $0.2 < ML < 4.1$ range) consists of a similar percentage of isotropic (implosive) and deviatoric components, with a normal fault-type best double-couple (DC).

We have also calibrated the regional stations for seismic coda-derived source spectra and moment magnitude using the envelope methodology of Mayeda et al. (2003). We tie the coda Mw to independent values from waveform modeling. The resulting coda-based source spectra of shallow mining-related events show significant spectral peaking that is not seen in deeper tectonic earthquakes. This coda peaking may be an independent method of identifying shallow events and is similar to coda peaking previously observed for Nevada explosions, where the frequency of the observed spectral peak correlates with the depth of burial (Murphy et al., 2008).

OBJECTIVES

The main objective of this project is to develop and exploit a unique seismic data set from mine-related events recorded at in-mine (<3 km), local (3–10 km), and regional (>100 km) distances (Figure 1). The in-mine recordings are being obtained through three in-mine seismic networks consisting of a few tens of high-frequency geophones (natural frequencies of 4.5 Hz, 14 Hz, and 28 Hz), which are routinely used to monitor seismic activity in the mines. The local recordings are being acquired through four broadband seismic stations (three Guralp CMG-3T and one Guralp CMG-40T feeding 24-bit RefTek data loggers) deployed under this project and located on the surface of the mining area. And the regional recordings are being acquired mostly through the AfricaArray stations in South Africa and surrounding countries. The dataset that we are assembling is unique in that it contains (1) events spanning several orders of magnitude, (2) events from a range of source depths, and (3) events from a variety of source types (e.g., pillar collapses, tensile fractures, normal and strike-slip faulting, and sources with a significant volumetric component).

We plan to exploit this dataset by using the mining events in 10 related areas of research aimed at improving U.S. operational capabilities to monitor for low-yield nuclear tests: (1) create an event catalog with accurate origin times and locations; (2) determine seismic moment, radiated energy, corner frequency, and stress drop; (3) obtain focal mechanisms from moment tensor inversion; (4) define several categories of event types (shear slip, tensile failure with volumetric component, explosions, pillar collapse) using focal mechanisms and in-mine observations; (5) define and calibrate a coda Mw scale for southern Africa; (6) using calibrated coda techniques, determine Mw for all cataloged events; (7) investigate the effects of depth and source mechanism on the coda-derived source spectra and evaluate the potential of using coda spectral peaking as a depth discriminant; (8) define and calibrate local-to-regional phase (direct P and S, Pn, Pg, Sn and Lg) propagation characteristics, including the use of the MDAC technique to determine appropriate geometrical spreading and frequency dependent Q values for the region; (9) characterize relative P and S excitation and source apparent stress resulting from variations in source parameters, including magnitude, mechanism, depth, rock characteristics, and source type; (10) define regional phase ratios that can discriminate between the different source categories, and compare these discriminants and their performance with ongoing work done for other types of mining events, such as in Scandinavia and the western U.S.

The first surface-mine broadband station was deployed in January 2007, and three more stations were deployed during the remainder of 2007, which have been operating continuously after installation. High-frequency recordings from the in-mine networks at Savuka, Mponeng, and TauTona have been already assembled for 2007 (January through December). The assembled data set contains tens of thousands of events spanning ~8 orders of magnitude (11,224 events in the $-3.4 < ML < 4.4$ magnitude range for Savuka), as catalogued by Integrated Seismic Systems International (ISSI), with high-quality broadband recordings at local distances (surface-mine network) for positive magnitudes ($ML > 0$) and regional distances for magnitudes above ML ~3.5. During this year, we have concentrated on quality control of the data (seismic locations and sensor orientations), as well as analyzing the in-mine recordings to develop a "ground-truth" database of robustly constrained locations, origin times, and full moment tensor solutions. We have devised automated procedures that check the inner consistency of the event associations provided by ISSI as well as the orientation of the in-mine sensors. We have also implemented an automated procedure to measure spectral amplitudes of P-, SV-, and SH-phases. We are now testing procedures to relocate seismic sources with the in-mine network and to obtain full moment tensor solutions from the spectral amplitudes. The procedures have been tested on the data set collected for 2007 at Savuka mine and are detailed in the next section.

In the coming year, we will continue assembling a similar data set for 2008 and applying the quality check (QC) procedures to all the in-mine data. We will refine the relocation and moment tensor inversion procedures and build a catalog of "ground-truth" seismic locations and moment tensors by comparing our seismic location and moment tensor solutions to detailed mine plans.

RESEARCH ACCOMPLISHED

Hypocentral Locations and Origin Times

Hypocentral locations for mine-related seismic events are routinely determined and reported by ISSI from manually picked P- and S-wave travel times on the in-mine recordings. Any event with at least four P-wave travel times and four S-wave travel times will be located by ISSI; otherwise, the event is rejected and not saved in the system. The locations are determined by inverting the picked travel-times after assuming a constant seismic velocity between the station and the seismic source; this velocity, however, can vary among stations for the same event in an attempt to

account for site effects within the mine. The inverted hypocentral locations and origin times are routinely reported by ISSI, along with basic source parameters such as P- and S-wave scalar moment, energy, and corner frequency.

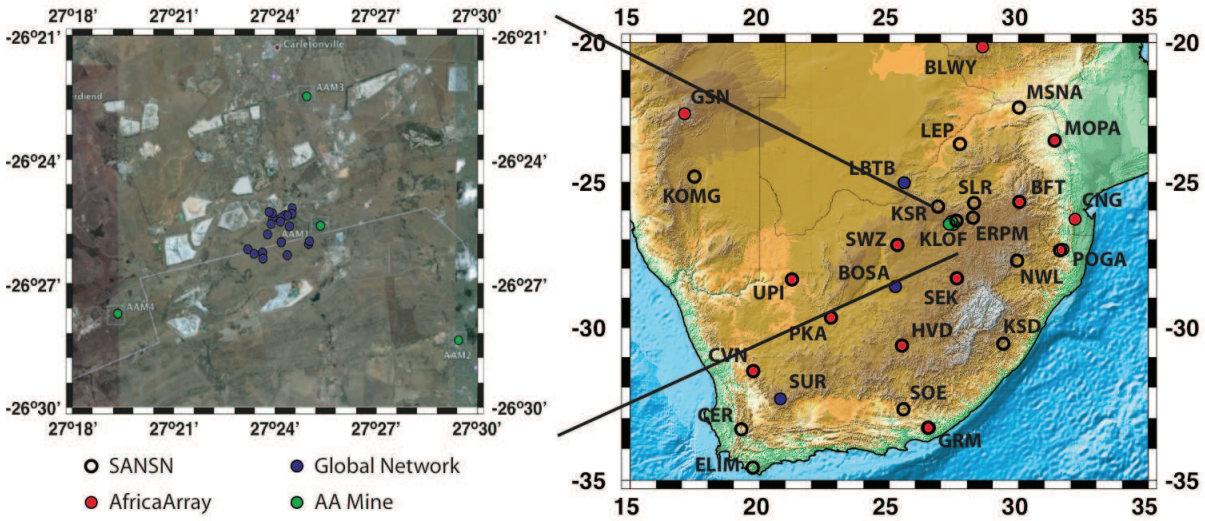

Figure 1. (left) Satellite image from Google Earth showing the Carletonville mining area where the three mines contributing to this project are located. The blue dots are the surface projection of the Savuka in-mine network, while the green dots are the surface broadband stations deployed under this project. (right) Map of broadband stations in South Africa. The red dots are the AfricaArray stations, which are shared with the South Africa National Seismic Network (SANSN), shown as open circles. The blue dots are the three permanent global seismographic network (GSN) stations.

In a recent visit to ISSI, we learned that the "dumping" command in their home-grown software erroneously writes the trigger time of the first seismic waveform recorded by the system in place of the event origin time. In order to obtain proper origin time estimates, we constructed Wadati diagrams for all the catalogued events. Wadati diagrams are plots of t_S-t_P versus t_P, where t_P and t_S are the P- and S-wave travel times, respectively. Under the assumption of a medium of constant velocity, it can be shown that

$$t_S - t_P = (V_P/V_S - 1)(t_P - t_o) ,$$

where t_0 is the origin time, and V_P and V_S are the P- and S-wave velocities, respectively. This is the equation of a straight line with a slope directly related to the V_P/V_S ratio of the propagating medium and which intersects the abscissa at the origin time.

Interestingly, we found that many times some (t_S-t_P,t_P) pairs did not fall on the Wadati line (see Figure 2). The travel-time differences are in general too large to be attributed to variations in seismic velocity, and are more likely caused by erroneous S-wave travel-time picks, false GPS locks or drifts in the timing system, phase misidentification, or erroneous event associations. The Wadati diagrams showed promise in successfully identifying these inconsistencies, and we devised an automated filter that extracts the largest subset of (t_S-t_P,t_P) pairs that follow a straight line (i.e., regression coefficient of 0.9 or larger) with an associated V_P/V_S ratio between 1.60 and 1.70. After applying this Wadati filter to the 11,224 catalogued event, a total of 2,508 were rejected. Those were mostly small events, generally with local magnitudes below 1.0, recorded at just a few stations (a minimum of 3 points are required in the Wadati filter to fit a straight line).

The results of this Wadati filter prompted us to relocate the events that passed the filter. We followed a very simple scheme in which the selected P- and S-wave travel times were inverted, assuming a whole space of $V_P = 6.1$ km/s and a $V_P/V_S = 1.64$. The forward problem is expressed as

$$t_P = t_0 + d/V_P \text{ and}$$

$$t_S = t_0 + d/V_S ,$$

where d is the hypocentral distance, and the relocation is done iteratively through the linearized scheme described by

$$\begin{bmatrix} \Delta t_1 \\ \Delta t_2 \\ : \\ \Delta t_N \end{bmatrix} = \begin{bmatrix} 1 & -(x_1-x_0)/d_1V & -(y_1-y_0)/d_1V & -(z_1-z_0)/d_1V \\ 1 & -(x_2-x_0)/d_2V & -(y_2-y_0)/d_2V & -(z_2-z_0)/d_2V \\ : & : & : & : \\ 1 & -(x_N-x_0)/d_NV & -(y_N-y_0)/d_NV & -(z_N-z_0)/d_N \end{bmatrix} \begin{bmatrix} \Delta t_0 \\ \Delta x_0 \\ \Delta y_0 \\ \Delta z_0 \end{bmatrix}$$

The iterative process was stopped when the change in the rms error was less than 1% or when the number of iterations was equal to 10. The latter situation occurred only for 22 events, which were rejected.

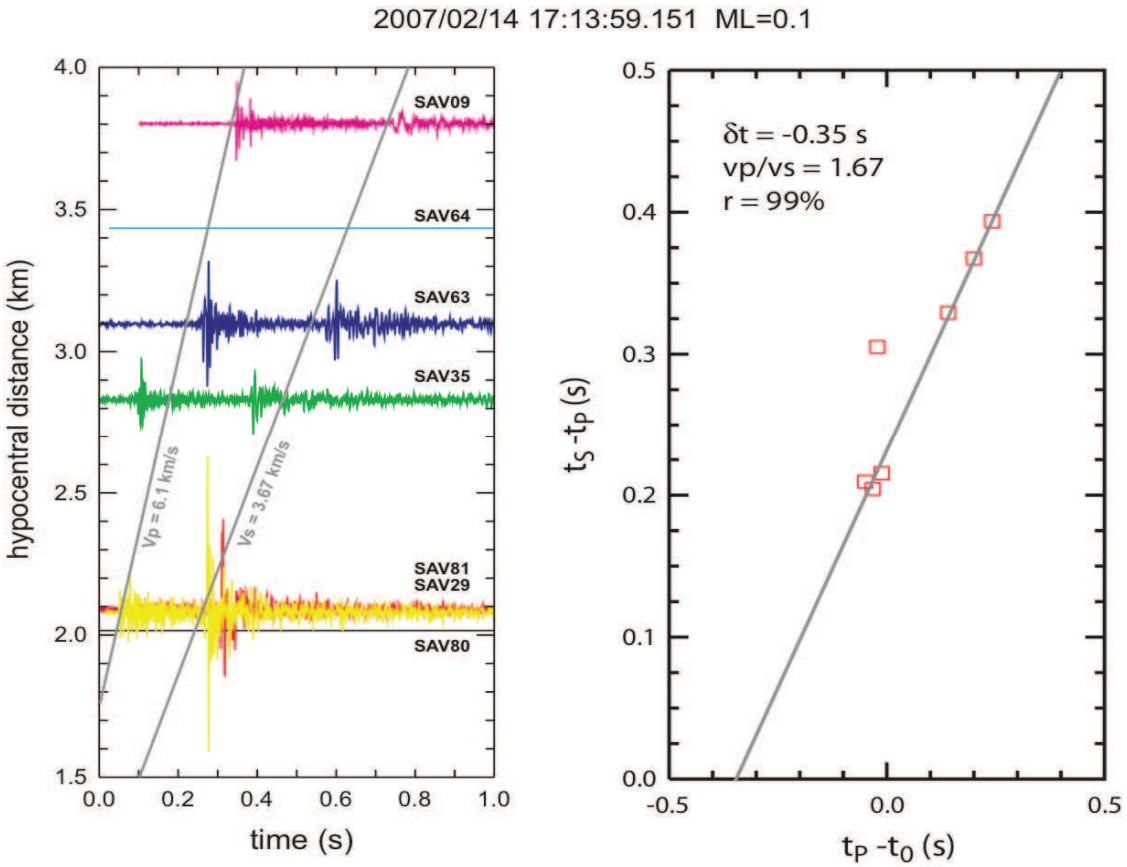

Figure 2. (left) Record section for a ML = 0.1 event (vertical traces) as recorded at the Savuka mine. Note that some traces (SAV64, SAV80) have a failed component and the time shift of trace SAV35. (right) Wadati diagram for the same event. Note how the point for SAV35 plots outside the Wadati line. The grey line is the LSQ fit to the points and has an associated Vp/Vs of 1.67, a correlation coefficient of 0.99, and an origin time correction of –0.35 s.

Figure 3A shows the distribution of rms differences between observed and predicted travel times before and after the relocation. The multimodal appearance of the "before" distribution is likely due to the trigger times erroneously reported as "origin times" by ISSI. Figures 3B–D display a few histograms summarizing the relocation procedure described above and show that, in general, the hypocenters migrated just a few hundred meters from the original ISSI location and that the original "origin times" needed a negative correction of a few tenths of second. Finally, note that origin time corrections were also obtained from the Wadati diagrams. Figure 3E shows that the corrections independently obtained through the Wadati diagrams and the relocation scheme are equivalent.

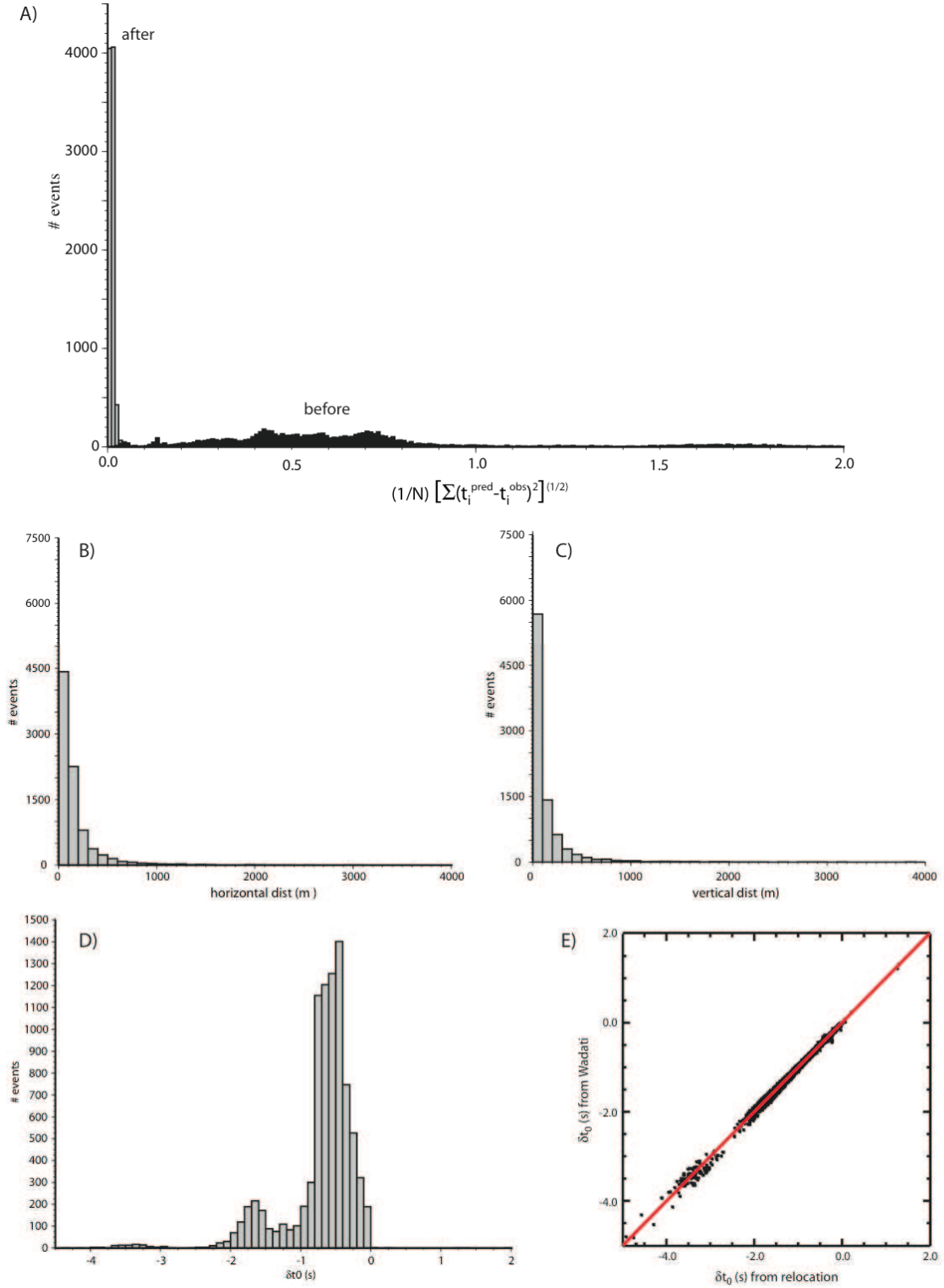

Figure 3. (A) Comparison of the distribution of travel-time residuals before and after relocation. (B) Histogram showing horizontal migration of hypocenters after relocation. (C) Histogram showing vertical migration of hypocenters after relocation. (D) Histogram showing origin time corrections after relocation. (E) Comparison between origin time corrections from the relocation scheme and from the Wadati diagrams.

Sensor Orientations

Seismic waveforms are originally recorded by the high-frequency geophones in the West, South, Down coordinate system. As a preliminary step to moment tensor inversion, the original traces must be rotated into the local ray-coordinate system (i.e., P, SV, SH). Such a rotation can be easily achieved from known hypocentral (x_0,y_0,z_0) and station locations (x_S,y_S,z_S) through

$$\text{tg } \varphi = (x_S - x_0)/(z_S - z_0)$$

$$\cos \theta = (z_S - z_0)/[(x_s - x_0)^2 + (y_S - y_0)^2 + (z_S - z_0)^2]^{1/2},$$

where x is North, y is East, and z is Up, and θ and φ are the take-off angle and azimuth, respectively. Due to the difficulties in installing and maintaining an in-mine network, however, half of the 20 high-frequency geophones making up the Savuka in-mine network had at least one failing component and could not be rotated (and used to constrain the moment tensor solutions). Moreover, many times the theoretical rotation lead to counter-intuitive results where most of the P-wave energy is polarized in the SH component, suggestive of a sensor misalignment.

The rotation angles can also be obtained empirically from the eigenvectors associated to the eigenvalues in the covariance matrix (Montalbetti and Kanasewich, 1970) defined as

$$\begin{pmatrix} \text{Var}[x] & \text{Cov}[x,y] & \text{Cov}[x,z] \\ \text{Cov}[x,y] & \text{Var}[y] & \text{Cov}[y,z] \\ \text{Cov}[x,z] & \text{Cov}[y,z] & \text{Var}[z] \end{pmatrix}$$

where,

$$\text{Var}[x] = \Sigma (x_i - x)^2/(n-1), \quad \text{Cov}[x,y] = \Sigma [(x_i - x^*)(y_i - y^*)]/(n-1) ,$$

where * denotes the average within the P-wave window on the in-mine recordings. Realize that this "polarization filter" successfully finds the directions of the P-, SV-, and SH-axis (Figure 5) but cannot resolve the sense of motion, due to the symmetry of the covariance matrix with respect to reflections about the origin of coordinates.

In any case, we systematically computed the correlation coefficients (absolute value) between the empirically and theoretically rotated P-, SV-, and SH-waveforms for each of the 8,000 relocated events. The results are displayed in Figure 4 and show that only 4 of the 9 stations are correctly oriented. We explored the possibility of a sensor misalignment due to a rotation about the vertical channel, and found that a clockwise rotation of ~55^o for SAV35, a rotation of 180^o for SAV34, and a clockwise rotation of 90^o for SAV77 and SAV79 led to the expected correlation coefficients between empirically and theoretically rotated waveforms. Unfortunately, no corrections could be found for SAV08 and SAV27.

We also checked sensor orientations for the surface-mine stations by comparing recordings of teleseismic waveforms with those recorded at the nearby GSN station LBTB, and found that station AAM3 had a rotation about the vertical channel of ~180^o.

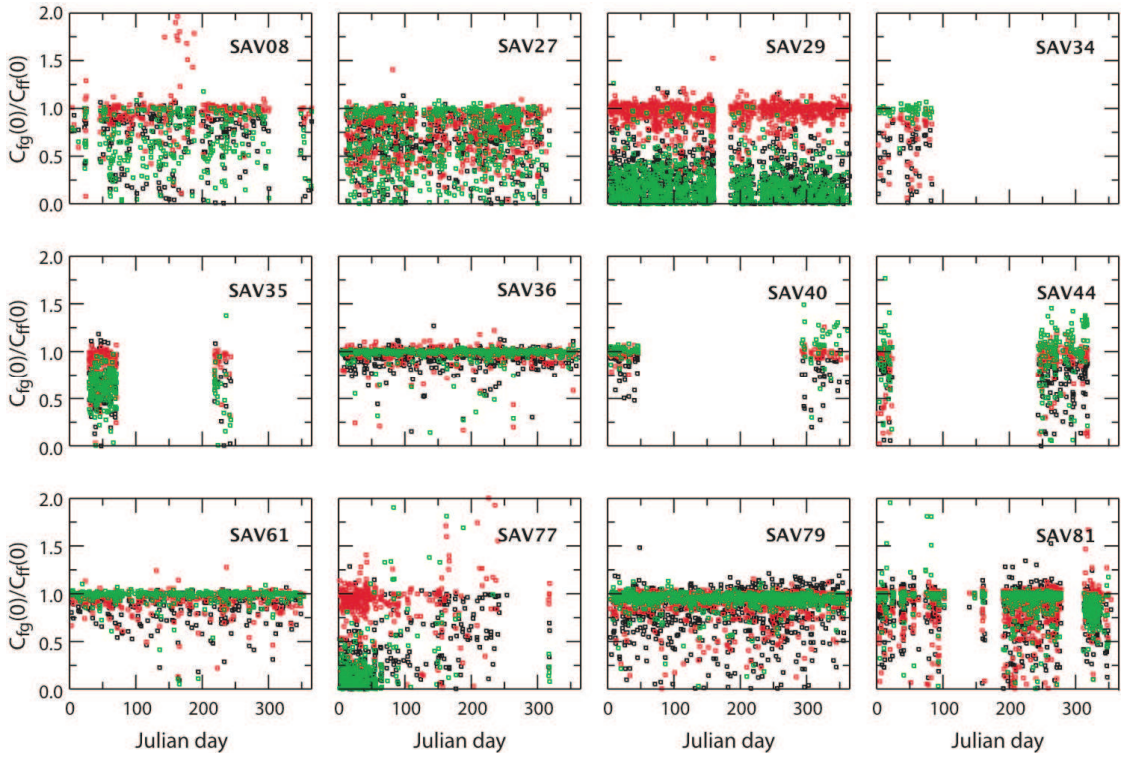

Figure 4. Correlation coefficients between theoretically and empirically rotated waveforms (green, SH; red, SV; black, P). Note that only stations SAV36, SAV40, SAV61, SAV79, and SAV81 show coefficients close to 1 in all three components.

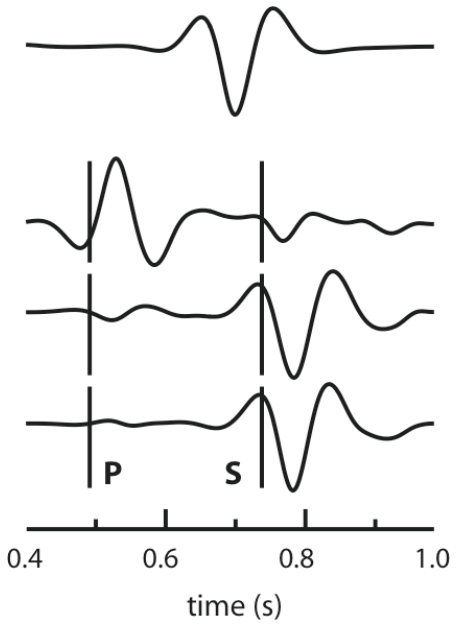

Figure 5. Impulse response for a 4.5-Hz instrument in the time-domain (top) and P-, SH-, and SV- recordings (bottom) of a mine-related event from station SAV29. Polarities can be assigned as negative (P), positive (SH), and positive (SH) after a visual comparison of the traces with the impulse response.

Moment Tensor Solutions

Full moment tensor solutions are being obtained from P-, SV-, and SH-spectral amplitudes. We assume a medium of uniform velocity (V_P = 6.1 km/s, V_P/V_S = 1.64), so that the displacements can be expressed as (e.g., Udías, 2000):

$$u_i = G_{ij,k} m_{jk} \quad i,j,k = 1,2,3 ,$$

where

$$G_{ij,k} = (1/4\pi\rho v^3 R)\, \gamma_i\gamma_j\gamma_k\, \delta'(t-R/v) \quad \gamma_i = x_i/R ,$$

where ρ is density, v is the P- or S-wave velocity, and R is the hypocentral distance. The forward problem is then written by rotating the displacements into the ray-coordinate system and Fourier transforming the resulting equation to obtain spectral amplitudes. This defines a linear problem that is inverted by calculating the natural inverse (e.g., Menke, 1989) through a singular value decomposition of the forward problem's matrix.

Spectral amplitudes from the in-mine recordings are obtained through the time-domain procedure of Urbancic et al. (1996). This procedure evaluates the spectral plateau of the P- or S-wave spectrum by computing the ratio

$$\Omega_o = 4(S_{D2})^{3/2}(S_{V2})^{-1/2} ,$$

where

$$S_{D2} = 2\int D^2(t)\, dt \quad S_{V2} = 2\int V^2(t)\, dt ,$$

and D(t) and V(t) are the displacement and velocity, respectively. Following Trifu et al. (2000), the integrals extend between the P- and S-wave travel-times, for the P-wave amplitude, and twice the S-P time after the S-wave travel time for the SV and SH amplitudes.

The polarity of the spectral amplitudes is assigned visually for each measurement. An impulse response is first generated in the time-domain for the sensor recording the amplitudes and then both the impulse response and the data are low-pass filtered at 10 Hz (or higher frequency for the 14-Hz and 28-Hz sensors). Due to the narrow frequency band of the resulting signal the side lobes are significant, but the final pulse shapes are generally good enough for assigning polarities (Figure 5).

Figure 6 (left) shows an example of a full moment tensor inversion for a Mw = 1.0 event recorded by the Savuka in-mine network. The moment tensor solution has a significant volumetric component (~60% implosive) and a deviatoric component that splits in similar amounts between double-couple (DC) and compensated linear vector dipole (CLVD) contributions. The best-fitting DC is of normal-fault type. Figure 6 (right) compares the low-pass filtered waveforms with synthetic waveforms for a whole space, to ensure the consistency between the time-domain and the frequency-domain amplitude measurements both in size and polarity. Even though we did not invert the waveforms in the time domain, the agreement is generally excellent.

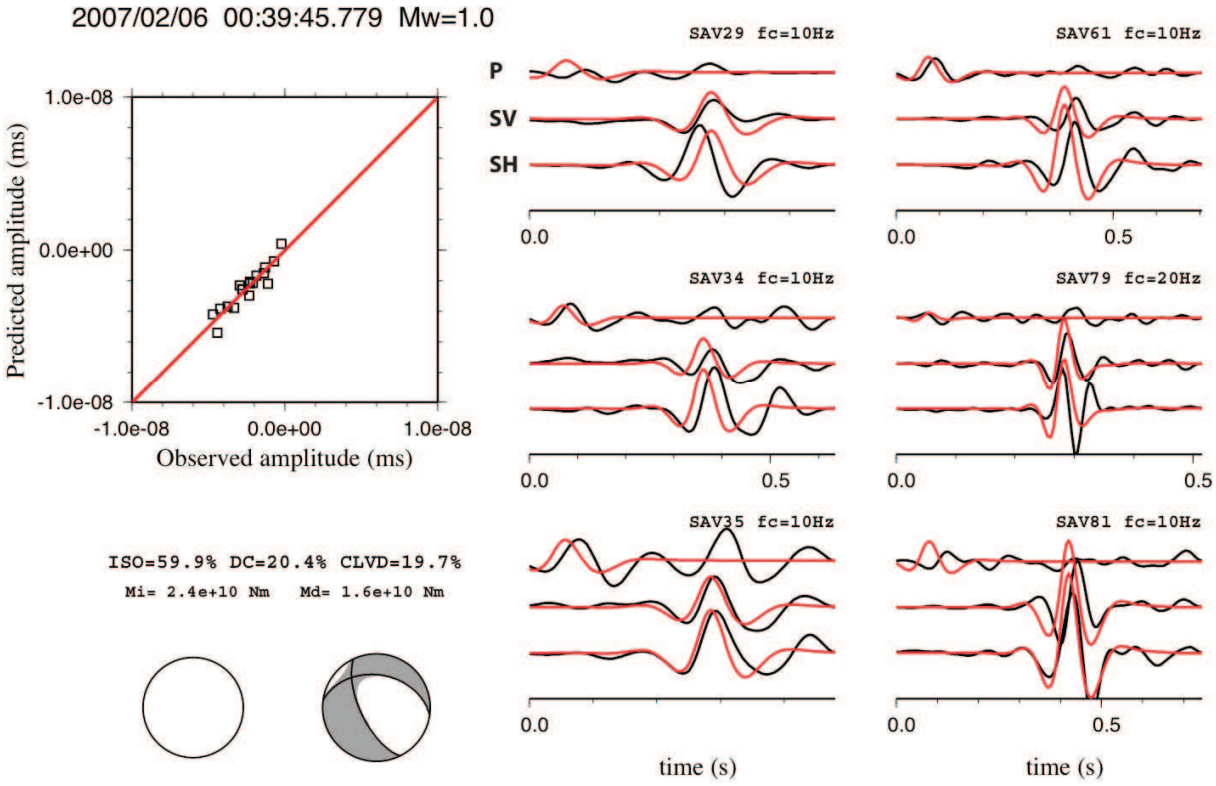

Figure 6. Moment tensor inversion results for a Mw=1.0 event recorded at Savuka mine. (left) Comparison between observed and predicted spectral amplitudes and isotropic and deviatoric "beach balls" for the moment tensor. (right) Comparison of observed (black) and predicted (red) waveforms. Realize the inversion was done with spectral amplitudes, not waveform inversion.

Regional Coda Magnitudes and Spectra

We have also been looking at the seismic coda from regional events, both natural earthquakes and mine-related, that are recorded at regional stations across South Africa. Regional coda envelopes are useful to establish a calibrated moment magnitude scale for the area and to study source spectra of events using the methodology of Mayeda et al. (2003). To calibrate the stations, we first examined the coda from events that are known to be natural earthquakes. In 2006 there was a magnitude 7.2 earthquake in Mozambique, just northeast of South Africa, that had a good sequence of aftershocks. We used this sequence and a few other earthquakes to determine the coda path and shape correction factors. By waveform modeling some of the largest events at intermediate periods, we obtained calibration moments and were able to derive the source spectra shown on the left hand side of Figure 7. These coda parameters can now be used to obtain moment magnitudes for any event recorded at one of the calibrated regional stations.

When we applied the coda technique to the mining-related events, we found unusual shaped source spectra with a peak amplitude near 1 Hz, as shown on the right hand side of Figure 7. Our working hypothesis is that the peaking is related to strong Rg excitation for the shallow mine-related events. We are working to better quantify these observations by looking at the good ground-truth location and depth mine events. This South African observation is similar to coda peaking previously observed for Nevada explosions, where the frequency of the observed spectral peak correlates with depth of burial (Murphy et al., 2008). These observations appear to indicate that coda spectral peaking might be used to identify shallow events and discriminate them from more-typical-depth earthquakes.

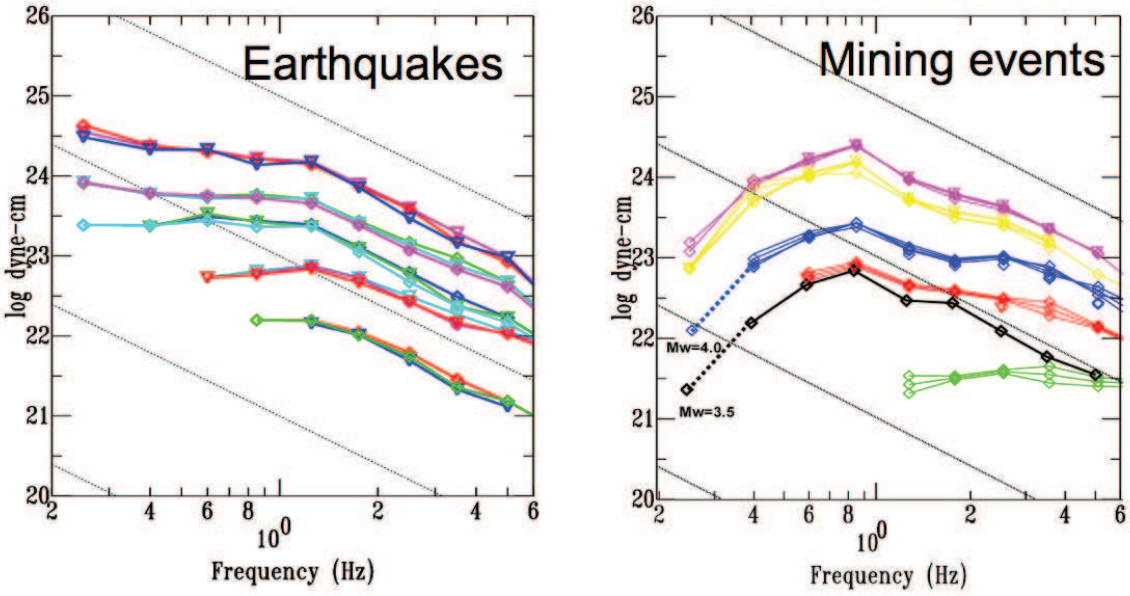

Figure 7. Coda derived source spectra from earthquakes (left) and mining induced events (right). The earthquakes have the usual shape: a near constant proportional to the moment at long periods and falling of as frequency^{-2} at the high frequencies. Coda based Mw's for any event can be determined from the long period level. In contrast the mine events show an unusual peaked shape, which may be an indicator of shallow depth due to Rg excitation and scattering into the coda. The lowest frequency points shown with dashed lines come from long period waveform modeling.

CONCLUSIONS AND RECOMMENDATIONS

1. The comparison between our event relocations and the original ISSI event locations (Figures 4b and 4c) suggest our estimates might be correct within a few hundred meters. ISSI claims their locations are accurate within ~50 m, but the outliers usually present in the Wadati diagrams suggest the accuracy could be lower. We are working with scientists at the Council for Industrial and Scientific Research (CSIR) in South Africa to implement a hybrid relocation scheme to produce more accurate locations (Spottiswoode and Linzer, 2003). In any case, an accuracy of a few hundreds of meters (i.e., ground truth 1, GT1) for the mine-related events is good enough for most of the areas of research aimed in this project.
2. The trigger times of the first recording stored in the in-mine network were erroneously reported as event origin times reported by ISSI. We have obtained consistent corrections from Wadati diagrams and a simple relocation scheme.
3. We have identified a few sensor misalignments for both in-mine and surface-mine stations. Corrections could be obtained for most of them by comparing empirical and theoretical rotations to the local ray-coordinate system, but some in-mine sensors still remain uncorrected.
4. Measurement of spectral amplitudes in the time domain has been successfully automated, but assigning polarity to the amplitudes is still done visually. We are still working on a procedure to automatically assign polarities.
5. We have obtained 111 moment tensor solutions for which 82 show a good match between observed and predicted amplitudes. The majority of these solutions (47 out of 82) have similar percentages of volumetric (implosive) and deviatoric component, in good agreement with the stress field expected from mining practices.

6. We have requested mine plans for 2007 for Savuka, Mponeng and TauTona. The mine planes will be critical in providing a "ground truth" check for our hypocentral locations and moment-tensor solutions.
7. Coda derived source spectra may provide a means of identifying shallow events and discriminating them from more normal-depth earthquakes. We are working to better understand and quantify this observation.

ACKNOWLEDGEMENTS

We thank ISSI and Anglo Gold Ashanti for providing the seismic data and mine plans from the Savuka, Mponeng and TauTona mines. We also thank ISSI and the Council for Scientific and Industrial Research for assisting with event locations and solving other technical issues concerning the in-mine data, and we thank the Council for Geoscience for installing and operating the four broadband stations of the surface mine network. The IRIS data management center has provided assistance with archiving and distributing data from the permanent AfricaArray seismic stations, including data used in this study.

REFERENCES

Mayeda, K., A. Hofstetter, J. O'Boyle, and W. R. Walter (2003). Stable and transportable regional magnitudes based on coda derived moment-rate spectra, *Bull. Seism. Soc. Am*. 93: 224–239.

Menke, W. (1989). *Geophysical Data Analysis: Discrete Inverse Theory*. Academic Press.

Montalbetti, J. M. and E. R. Kanasewich (1970). Enhancement of teleseismic body waves with a polarization filter, *Geophys. J. R. Astr. Soc.* 21: 119–129.

Murphy, K. R., K. Mayeda, and W. R. Walter (2008). Lg-coda methods applied to Nevada Test Site events: Spectral peaking and yield estimation, submitted to *Bull. Seism. Soc. Am.*

Spottiswoode, S. and L. Linzer (2003). Improved seismic event locations, *ISRM 2003: Technology Roadmap for Rock Mechanics* 1–6.

Trifu, C. I., D. Angus, and V. Shumila (2000). A fast evaluation of the seismic moment tensor for induced seismicity, *Bull. Seism. Soc. Am.* 90: 1521–1527.

Udías, A. (2000). *Principles of Seismology*. Cambridge University Press.

Urbancic, T. I., C. I. Trifu, R. A. Mercer, A J. Feustel, and J. A. G. Alexander (1996). Automatic time-domain calculation of source parameters for the analysis of induced seismicity, *Bull. Seism. Soc. Am.* 5: 1627–1633.